# Solid State NMR Spectroscopic Investigations of Model Compounds for Imidazole-Based Proton Conductors

**Ingrid Fischbach**

*BASF AG, Polymer Research, Department of Polymer Physics, 67056 Ludwigshafen, Germany*

**Hans Wolfgang Spiess**

*Max-Planck-Institut für Polymerforschung, Postfach 3148, D-55021 Mainz, Germany*

**Kay Saalwächter**

*Institut für Makromolekulare Chemie, Universität Freiburg, Stefan-Meier Str. 31, D-79104 Freiburg*

**Gillian R. Goward***

*Department of Chemistry, McMaster University, 1280 Main St. W., Hamilton, ON, L8S 4M1 Canada*

*Received: July 15, 2004; In Final Form: September 7, 2004*

The temperature dependence and the exact geometry of slow molecular reorientations in imidazolium methyl sulfonate are investigated using modern one-dimensional MAS exchange spectroscopy. Earlier high-temperature studies have evidenced a fast 180° flip motion of the imidazole ring, which is shown here to slow on cooling and is believed to be a prototypical molecular process involved in Grotthus-type proton transport in imidazole-based proton conductors intended for fuel cell applications. It is further shown that valuable information on the relative orientations of CH and NH dipolar coupling tensors with respect to the chemical shift anisotropy tensors of the respective heteronuclei can be obtained from the MAS exchange data as well as from static $^{13}C$ and $^{15}N$ line shapes, without the necessity of performing more involved single-crystal NMR experiments. The principal axes of the CSA tensors are found to not coincide with the CH or NH bond axes, in contrast to earlier assumptions involving similar compounds. Imidazole itself is shown to be more complex than might be expected, based on its simple structure. Implications on earlier studies of pure imidazole, where ring flips were claimed to be absent, are discussed.

## Introduction

Imidazole and polymers derivatized with imidazole or similar heterocycles have attracted attention recently as proton-conducting materials with potential applications as membrane materials in polymer electrolyte membrane fuel cells (PEM-FCs).[1,2,3,4] In developing new materials for these applications, tethered imidazole rings offer the opportunity for high-temperature conductivity, with the imidazole acting as a proton solvent. The primary advantage of such materials is that the proton solvent will not evaporate from the fuel cell under high-temperature conditions, in contrast to the classic Nafion and other acid-functionalized polymers, which are water-based systems.[5] Within this emerging class of materials there remain many unanswered questions regarding the mechanisms of proton transport, and, moreover, regarding how to mitigate factors that impede conductivity. In this investigation, we complete an in-depth probe of the properties of imidazolium methylsulfonate, a model compound for the more complex polymeric systems.

Using high-resolution $^{1}H$ solid state NMR, we have characterized proton mobility in a family of ethylene-oxide-tethered imidazole rings, Imi-nEO.[6] In our ongoing physical characterization of conductivity and mobility in such materials, we identified ring reorientations in imidazolium methylsulfonate.[7] This salt is a model compound for the acid-doped membrane materials, in which methylsulfonic acid, or the perfluorinated analogue, triflic acid, would be preferred dopants. These acids have large anions that are limited sterically with respect to diffusion. Thus, under an applied potential, the more probable case is that the proton would diffuse via the Grotthus or structural diffusion mechanism, promoting ionic conductivity of the electrochemically relevant ion.[8]

We found that imidazolium methylsulfonate exhibits molecular reorientations within the crystalline solid below the melting temperature.[7] Such behavior is well documented in a variety of molecular crystals and is considered a desirable feature of ionic conductors for electrochemical applications.[9,10,11] We hypothesized that ring reorientation in imidazolium methylsulfonate is the rate-limiting step for proton transport in imidazole-based materials. This has also been proposed by other groups working on theoretical investigations of imidazole itself.[12,13,14] Our previous investigations were based on analysis of $^{13}C$ coalescence, as well as the influence of the local motion on $^{1}H-^{13}C$ dipolar side band patterns,[15,16] recorded using REDOR-based heteronuclear recoupling techniques (REPT, recoupled-polarization transfer), and yielded 38 kJ/mol as a first estimate for the activation energy of the process.[7] The dipolar side band patterns showed an averaging of the basal $^{13}C$ resonances, whereas the

* Corresponding author: Prof. Gillian R. Goward. Tel: (905)525-9140 x24176. Email: goward@mcmaster.ca.

10.1021/jp046848h CCC: $27.50 
Published on Web 11/09/2004

apical resonance was influenced to a much lesser extent. This behavior was attributed to a two-site ring reorientation about the $C_2$ axis of the imidazolium rings.[7]

To obtain a more quantitative picture of the ring reorientation, we present here our in-depth investigation of both the slow time dependence of the molecular process in the temperature regime between 300 and 380 K, as well as the geometrical constraints for the motional process, as a complement to our previous study.[7] For these purposes, we employed the CODEX (*c*enter-band-*o*nly *d*etection of *e*xchange, pulse sequence), which probes molecular reorientation or exchange through the influence that the motion has on the chemical-shift anisotropy (CSA).[17] CODEX, one of the most powerful one-dimensional exchange NMR techniques, has previously been used to examine many types of molecular reorientations, including phenyl ring flips in polyaryl ethers,[18] hexabenzocoronenes,[19] rigid dendrimers,[20] as well as dynamics in poly(methyl methacrylate), and isotactic polypropylene.[17]

CODEX build up curves provide information on the geometry of a molecular process, and their interpretation requires accurate data on the CSA of the $^{13}$C nuclei. The $^{13}$C CSA tensors were analyzed with the SUPER (*s*eparation of *u*ndistorted *p*owder patterns by *e*ffortless *r*ecoupling) pulse sequence,[21] applied under MAS due to the overlap of the three $^{13}$C line shapes in a one-dimensional spectrum. Using SUPER, undistorted, quasistatic CSA powder patterns can be extracted for each isotropic chemical shift position in the $^{13}$C spectrum, providing all principal values of the $^{13}$C CSA tensors.

Further, the effects of motion on the $^{15}$N CSA tensor were analyzed directly by traditional static Hahn echo[22] measurement of the static $^{15}$N powder line shape. The combination of all our data provides conclusive evidence for the two-site ring reorientation observed in imidazolium methylsulfonate, as well as unique information on relative orientations of heteronuclear $^1$H−X dipolar and CSA tensors. Such data are notoriously difficult to obtain directly. Therefore, earlier $^{15}$N NMR studies concerned with molecular reorientations in imidazole and neutral and charged derivatives[10] relied on estimates based on quantum-chemical calculations,[23] which indicated that the principal axes should be, as expected, along the NH bonds. Our indirect determination employing the dynamics of the ring disproves this intuitive picture, at least for the special case of imidazolium methyl sulfonate.

Pristine crystalline imidazole has an extremely long spin−lattice relaxation time, $T_1$,[6,24,25] which has so far limited our studies of imidazole itself. Here, we present 1D $^{15}$N MAS NMR and $^1$H MAS and double-quantum filtered NMR data for imidazole. As well, we consider a series of photographs of the crystal, taken during X-ray diffraction experiments, which give some evidence as to the nature of this material.

Together, these studies have some implications on the heavily debated proton conduction mechanism in this compound and point toward a generalized understanding of the rate-limiting steps and proton-conductivity mechanisms in the wider class of imidazole-based materials.

## Experimental Section

The CODEX experiment is based on recoupling of the chemical shift anisotropy via two series of rotor-synchronized $\pi$ pulse trains flanking a mixing period and followed by a z-filter, both of variable length but fixed sum. The intensity difference between a reference spectrum and spectra with varying mixing times, normalized to the reference spectrum, is zero when no motion occurs and nonzero for a case in which a motional process has changed the chemical shift anisotropy during the mixing time, thereby precluding the formation of an echo by the second recoupling period. The characteristic time of the molecular process is extracted from the mixing-time dependence of the data at a fixed recoupling time, while the geometry of motion is inferred from the recoupling-time dependence at a fixed mixing time (so-called build up curve). The long-time plateau intensity further contains information about the number of sites accessible to the process and/or a fraction of immobile nuclei. Theoretical descriptions of the experiment are found in deAzevedo et al.[17] and Fischbach et al.[19] CODEX experiments were performed on a BRUKER DSX300 spectrometer operating at 300.23 MHz for $^1$H and at 75.49 MHz for $^{13}$C. The measurements were performed at a series of temperatures between 230 and 290 K, with a fully $^{15}$N-labeled sample packed in a 4 mm zirconia rotor spun at 10 kHz. The isotopic enrichment eliminated the possibility of additional dephasing due to the RIDER (*r*elaxation *i*nduced *d*ipolar *e*xchange with *r*ecoupling) effect.[26] CODEX parameters were as follows. Typical $\pi/2$ pulse lengths of 4 $\mu$s were used together with 2 ms cross-polarization . $^1$H dipolar decoupling at $\omega_{^1H}/2\pi \sim 80$ kHz was applied during the $\pi$ pulse trains, as well as during acquisition. Six loops of the $\pi$ pulse train were used before and after the mixing time. Mixing times were varied between 1 ms and 3 s.

The SUPER and static $^{15}$N experiments were performed on a BRUKER DSX500 operating at 500.12 MHz for $^1$H, 125.03 MHz for $^{13}$C, and 50.66 MHz for $^{15}$N using a 2.5 mm zirconia rotor as sample container. For the SUPER experiment, a spinning frequency of 7 kHz and a scaling factor $\chi' = 0.155$ was chosen, resulting in an effective spectral width in the indirect dimension of $\omega_R/\chi' = 45$ kHz. The offset was set in the middle between the two basal peaks at 118.7 ppm. For the $^{13}$C 360° pulses, the pulse strength was set to 85 kHz, according to $\omega_{^{13}C} = 12.12\omega_R$. Proton decoupling during the 360° $^{13}$C pulses was set to $\omega_{^1H}/2\pi \approx 150$ kHz.

The static $^{15}$N spectra were recorded with initial cross-polarization followed by a Hahn echo. The echo delay was 30 $\mu$s. The $^{15}$N chemical shift was referenced to glycine, which has a $^{15}$N chemical shift of −346.40 ppm with respect to nitromethane $CH_3NO_2$.

$^{15}$N MAS spectra of the imidazole sample were measured at a BRUKER DRX700 operating at 700.13 MHz for $^1$H and 70.93 MHz for $^{15}$N·spinning at 30 kHz. The $^{15}$N $\pi/2$ pulse length was set to 3.5 $\mu$s. During acquisition the TPPM scheme was applied for dipolar decoupling, using approximately 170° pulses and a phase-modulation angle of 30°.

$^1$H MAS spectra of imidazole were acquired at a BRUKER AV500 spectrometer operating at 500.13 MHz, under 30 kHz MAS. The $^1$H $\pi/2$ pulse length was set to 2.5 $\mu$s, and two rotor periods of excitation were used for the DQF spectra.

## Results and Discussion

**(a) Correlation Time and Energy of Activation.** CODEX experiments were performed in the temperature range 250−305 K (these are the *T*-corrected temperature limits.), with mixing times between 1 ms and 3000 ms. Selected mixing-time dependences of the normalized CODEX intensity for a series of temperatures are shown in Figure 1. The curves are fitted to biexponential functions. The first correlation time is associated with the imidazolium ring reorientation, and the rate is seen to increase steadily with increasing temperature, as is evident from the increasing initial slope. The initial plateau value in each case is roughly 35% and is observed to increase steadily

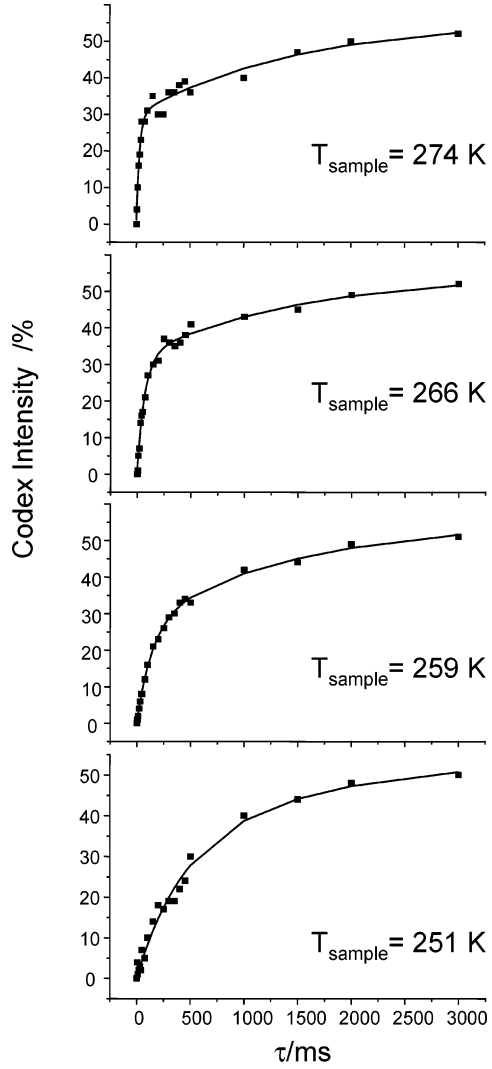


**Figure 1.** Mixing-time dependent normalized CODEX intensities for imidazolium methyl sulfonate obtained at sample temperatures of 251, 259, 266, and 274 K. The data were obtained under 10 kHz MAS spinning with a recoupling time of 0.6 ms, or six rotor periods. The data were fitted using a two parameter exponential function, with the second time held constant at 1500 ms.

toward 50% with increasing mixing times. A plateau at 50% exchange intensity would be consistent with a two-site jump process, as described by Schmidt-Rohr et al.[17] We attribute the deviation from 50% to a slightly short recoupling time of 0.125 ms, or 1.25 rotor periods, which was chosen to optimize the signal-to-noise ratio, since the signal deteriorates with extended recoupling times. Referring to the build up curve in Figure 4, which was acquired using a mixing time of 2 s, the expected 50% plateau is clearly reached for longer recoupling times, consistent with the expected 180° ring flip.

Considering the data in Figure 1, it is clear in each case that there is a gradual increase in the plateau value, at long mixing times, which is presumed to be driven by spin diffusion, or alternatively, by a RIDER effect.[26] As a side effect in any CODEX experiment, the heteronuclear dipolar coupling of $^{13}C$ to either $^{14}N$ or $^{15}N$ is recoupled, creating a spin state of the type $C_xN_z$. This state is stored along $z$ as $C_zN_z$ during the mixing time. Then, $T_1$ relaxation of the nitrogen (which is either dominated by quadrupolar coupling for $^{14}N$ or CSA for $^{15}N$) attenuates this term and precludes the formation of a full echo in CODEX, resulting in an apparent exchange effect. Having enriched the sample with $^{15}N$, we have eliminated the possibility

**TABLE 1: Parameters for Fits of CODEX Data for Various Temperatures**

| sample temp./K | $\tau_1$/ms | $\tau_2$ (fixed)/ms[a] |
|---|---|---|
| 274 | 29 ± 3 | 1500 |
| 266 | 70 ± 3 | 1500 |
| 262.5 | 78 ± 3 | 1500 |
| 259 | 149 ± 3 | 1500 |
| 255 | 192 ± 3 | 1500 |
| 251 | 392 ± 3 | 1500 |

[a] Second time was held constant, to account for spin diffusion, while the first time varied, according to the correlation time for ring reorientation.

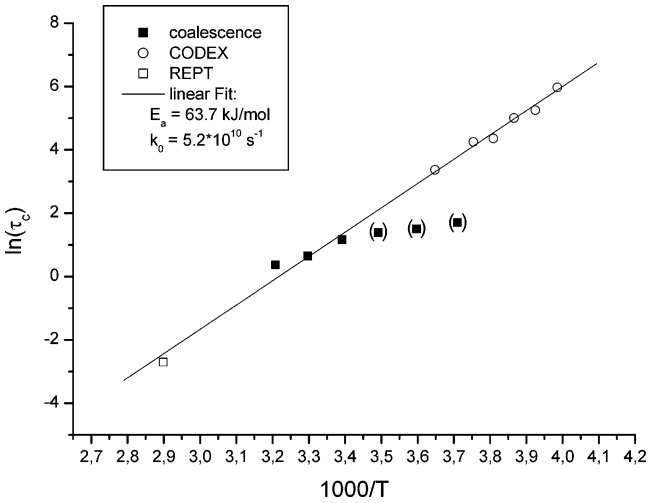


**Figure 2.** Correlation times for reorientation as a function of inverse temperature, extracted from three NMR experiments: REPT (open squares),[4] Coalescence (solid squares),[4] and CODEX (open circles). The activation energy for this process is determined to be 63.7 kJ/mol, excluding the three points in parentheses from the coalescence data. Apart from those points, a straight-line function with Arrhenius behavior is found, and thus all data represent the same two-site ring reorientation process.

of the former, which would be strong due to the rapid relaxation times typical of quadrupolar nuclei. To properly compare the influence of a RIDER effect, $^{15}N$ $T_1$ measurements would be necessary.

Spin diffusion among the $^{15}N$ is just as likely a reason for the increase of the plateau; it has been observed in comparable materials. The slow processes are in any case satisfactorily accounted for in each fit by fixing the second correlation time to 1500 ms. We have observed similarly efficient spin diffusion among naturally abundant $^{13}C$ in a recent study of polyphenylene dendrimers.[20] Spin diffusion, as well as $^{15}N$ $T_1$, should not change much with temperature in the investigated interval; therefore, this value is kept constant among the data sets. At temperatures above 274 K, the motion becomes too rapid to be accurately quantified using this pulse sequence. This is evident in the significant scatter that was observed among the data points at higher temperatures. Table 1 lists the fitted parameters for each CODEX data set.

In Figure 2, all the relevant correlation times, obtained from CODEX, REPT,[4] and coalescence measurements[4] are plotted together against inverse temperature. The resulting straight-line relationship is accurately described by a single Arrhenius function, consistent with a single two-site imidazolium ring reorientation process, measured by all methods. Only the coalescence points at low temperatures do not fit the Arrhenius curve, which can be attributed to the large experimental error suffered by these data points. We attribute the systematic error

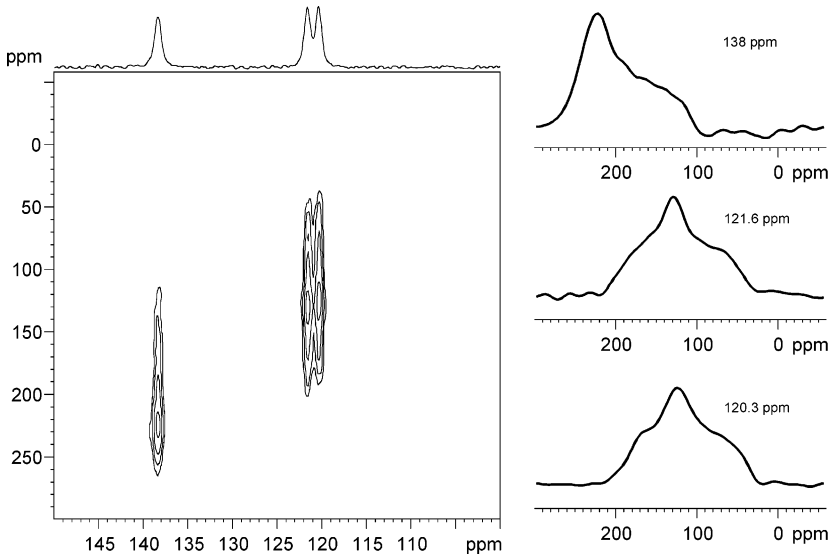


**Figure 3.** $^{13}C-$SUPER spectrum measured at $T = 265$ K. On the right, slices for the three aromatic resonances are shown. The spectrum was not subjected to the shearing procedure described in Liu et al.[21] The patterns were simulated with the weblab program[31] (grey lines), and the extracted tensor values are listed in Table 3 and were corrected according to their known isotropic chemical shift.

**TABLE 2: Activation Energies Determined from NMR Measurements and Impedance Spectroscopy, Corresponding to Microscopic and Macroscopic Measures of Proton Conductivity, Respectively**

| material | $E_A$ (NMR Data)/ kJ/mol | $E_A$ (NMR Data)/ kJ/mol doped with 10% triflic acid | $E_A$ (conductivity)/ kJ/mol |
|---|---|---|---|
| Imi-1EO[6] | 128 ($^1$H $T_2$) | N/A[a] | 48 |
| Imi-5EO[6] | 52 ($^1$H $T_2$) | N/A[a] | 60 |
| Imi-ms | 63 ($^{13}$C this paper) | N/A[a] | N/A[a] |
| PIm[27] | 44.8 ($^1$H $T_2$) | 26.7 | N/A[a] |
| CIm[27] | 47.4 ($^1$H $T_2$) | 23.5 | N/A[a] |

[a] N/A indicates values that are not available.

observed at low temperature to the changing effectiveness of heteronuclear decoupling as the time scale of the motional process changes. Since the heteronuclear decoupling directly influences the line widths, it is foreseeable that its influence will affect the coalescence data at low temperature, where the potentially distorted line widths are the dominant fitting parameter. At higher temperature, the changing chemical shift difference dominates, and the coalescence process becomes more unique.

The activation energy obtained excluding these three points is 63.7 kJ/mol and the preexponential factor is $k_0 = 5.2 \times 10^{10}$ kJ/mol. This value is notably higher than our earlier estimate of $E_A = 38 \pm 5$ kJ/mol, which was based on the coalescence data for this material. We are convinced that this discrepancy is due to the error in the low-temperature coalescence data points and, moreover, are able to interpret this high activation energy in terms of the chemistry of the material.

To understand the significance of this activation energy, it is helpful to compare it with values determined for other imidazole-based materials. Table 2 lists a comparison of activation energies for proton hopping, determined from $^1$H $T_2$ data, as well as activation energies for proton transport, determined by impedance spectroscopy. We note that the energy barrier for ring reorientation in imidazolium methylsulfonate is determined by the energy required to break two electrostatic, or Coulombic, interactions between the two N−H moieties of the protonated imidazole ring and the coordinating negatively charged sulfonate groups. The higher activation energy, as compared to the Imi-EO systems, is consistent with the stronger interactions in the salt, as compared to the hydrogen-bonding interactions in the molecular materials. In Imi-5EO, ring reorientation requires breaking and reforming two such hydrogen bonds. An additional difference between the Imi-EO oligomers and Imi-ms is the packing geometry. It is reasonable to assume that the tight packing geometry of the crystalline salt will sterically confine the imidazolium rings, also increasing the activation energy for ring flips. Therefore, the different activation energies arise from the relative strengths of the electrostatic interactions and the packing geometries of the two solids. We conclude that this rate-determining step will be critical to all imidazole-based proton conductors. In our ongoing studies, we investigate the observed drop in activation energy for siloxane polymers (PIm) and cycles (CIm), functionalized with Imi-EO side chains and doped with small amounts of triflic acid, which acts by disrupting the H-bonding network as well as inhibiting crystalline domain formation, thus lowering the energy barrier for ring reorientation relative to the pristine material.[27]

**(b) Geometry of Motion and Tensor Orientations.** Combining the results from the fast-limit averaging of $^1$H−$^{13}$C and $^1$H−$^{15}$N heteronuclear dipolar coupling tensors described in our previous study[4] and the information from the previous section that the process corresponds to a two-site jump, we can state that the imidazolium ring performs a 180° flip motion around an axis parallel to the apical C−H bond. We will now show that the analysis of the recoupling-time dependent CODEX intensities, in combination with CSA line shape measurements, allows us to deduce the orientation of the $^{13}$C and $^{15}$N CSA tensors in the molecular frame of the imidazolium ring.

For an analysis of the CODEX build up curve, the $^{13}C-$CSA tensor values need to be known. We determined them with the SUPER experiment,[21] which allows us to extract all three principal values of the CSA tensor in a site-resolved fashion. Figure 3 shows the SUPER spectrum of Imi-ms measured at $T = 265$ K. The obtained tensor values are listed in Table 3.

Figure 4 shows the CODEX build up curve of the basal carbon measured at $T = 259$ K, acquired with a mixing time of 2 s. Build up curves were calculated for various effective reorientation angles with the tensor values extracted from the SUPER experiment. The experimental build up behavior (dots) fits best to an effective reorientation angle of 27°, which

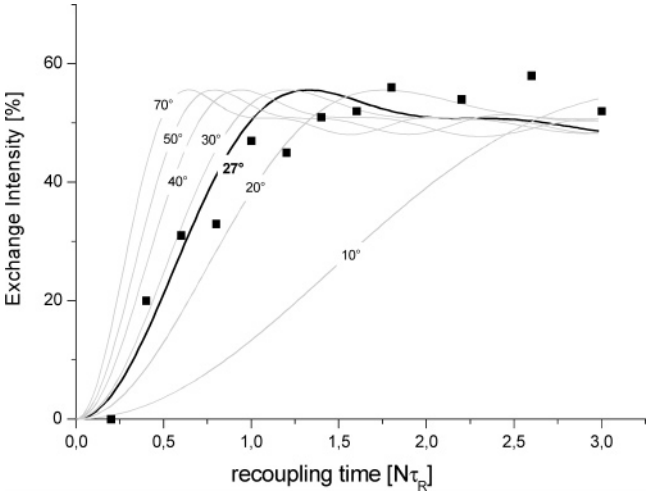


**Figure 4.** CODEX build up of the basal carbons measured at $T = 259$ K (dots). The solid lines are calculations for various flip angles. The black line corresponds to an effective flip angle of 27°, which fits the initial build up best.

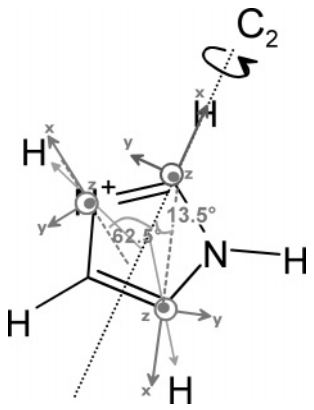


**Figure 5.** Sketch of the orientations of the PAS of the various CSA tensors in the molecular frame (gray coordinate systems). The *x* axis of the PAS of both the basal $^{13}C$ and the $^{15}N$ CSA tensor strongly deviates from the C−H and N−H bond direction, respectively. Only the *x* axis of the PAS of the apical carbon lies on the C−H bond, thus reflecting the $C_2$ symmetry at this carbon.

**TABLE 3: Three Principal Values of the CSA Tensor Obtained from the SUPER Experiment,[21] for All Three $^{13}C$ Resonances**

| position | $\sigma_{xx}$ | $\sigma_{yy}$ | $\sigma_{zz}$ |
|---|---|---|---|
| apical | 198 ± 5 | 168 ± 5 | 50 ± 5 |
| basal (121.6 ppm) | 196 ± 5 | 127 ± 5 | 42 ± 5 |
| basal (120.3 ppm) | 195 ± 5 | 125 ± 5 | 41 ± 5 |

corresponds to an angle of 13.5° between the $C_2$-symmetry axis (jump axis) and the *x*-principal axis of the $^{13}C$ CSA-tensor. This is very surprising, since the C−H bond encloses an angle of 35.6° with the $C_2$-symmetry axis. Obviously, the orientation of the $^{13}C$ CSA tensor is strongly counterintuitive. Usually, in aromatic systems, the *x* axis of the $^{13}C$ CSA tensor lies more or less on the C−H bond.[28] This is not the case here. The CSA tensor orientation is depicted in Figure 5.

To obtain further proof of this orientation, a SUPER experiment was performed at $T = 355$ K. At this temperature, the jump process is certainly in the fast limit, so the motionally averaged $^{13}C$−CSA tensor should be detected. At first sight, the result seems surprising, since the patterns (shown in Figure 6) are not significantly different from the low-temperature patterns (Figure 3). However, this fact is consistent with the small effective flip angle extracted from the CODEX build up behavior. With the rigid tensor values of $\sigma_{11} = 196$ ppm, $\sigma_{22} = 127$ ppm, and $\sigma_{33} = 42$ ppm and an effective flip angle of 27°, the averaged tensor can be readily calculated. One obtains for the motionally averaged tensor $\sigma_{xx} = 192$ ppm, $\sigma_{yy} = 133$ ppm, and $\sigma_{zz} = 42$ ppm, which is in good agreement with the experimental results. The pattern of the apical carbon also does not change, which is due to the fact that its CSA tensor is orientated in such a way that it is not affected by the flipping process.

The counterintuitive $^{13}C$−CSA tensor orientation is also supported by our own calculations of the CSA tensor, which yield an angle of 13.5° between the *x* axis of the PAS of the basal $^{13}C$ CSA tensor and the $C_2$ symmetry axis.[29] Further information on tensor orientations can be obtained from static $^{15}N$ spectra. Since the compound is isotopically enriched and exhibits only one $^{15}N$ resonance, site resolution and MAS are not mandatory. Hence, simple static Hahn echo spectra were recorded. Figure 7 shows the spectrum measured at 303 K together with a simulation using tensor values of $\sigma_{11} = -136$ ppm, $\sigma_{22} = -207$ ppm, and $\sigma_{33} = -342$ ppm. In Figure 8, a row of temperature-dependent Hahn echo spectra is shown. Clearly, the $\sigma_{33}$ tensor value is retained by the motional process. Only the $\sigma_{11}$ and $\sigma_{22}$ tensor values are averaged by the flip process. This again indicates a 180° flip as the only motional process. At a sample temperature of 353 K, the jump process is in the fast limit. From the averaged tensor values, the effective reorientation angle of the jump process can be determined, which directly translates to the orientation of the $^{15}N$ CSA tensor in the molecular frame. We found that an effective reorientation angle of 123° corresponding to an angle of 62.5° between the x PAS axis and the $C_2$ symmetry axis fits the fast limit pattern best. With the reorientation angle determined, it is now possible to calculate intermediate line shapes of the $^{15}N$ powder patterns to have an independent check of our result for the temperature dependence of the correlation time. On the right side of Figure 8, calculated patterns with correlation times taken from the Arrhenius plot in Figure 2 are shown. The trend in the calculated spectra reflects the trends in the experimental spectra. However, since the overall changes in the $^{15}N$−CSA tensor are too small, a fit of correlation times from the intermediate motional line shapes is too erroneous and hence was not carried out. Nonetheless, the $^{15}N$−CSA spectra clearly prove that it is the same motional process observed over the whole temperature range.

Here again, the orientation of the most deshielded CSA principal axis does not coincide with the NH bond. In an earlier study on imidazole and some derivatives,[23] $^{15}N$ CSA principal values were experimentally determined, but their orientation, allegedly along the NH bond in all cases, was only estimated from quantum-chemical calculations based on density-functional theory. These data were in turn the basis of a $^{15}N$ exchange study of possible flip motions in pristine imidazole.[10] Although these authors could not find evidence for a flip motion, we might hypothesize that an unexpected $^{15}N$ CSA orientation might have made their experiment insensitive to such a process.

To conclude this section, we have thus presented a protocol, entirely based on powder spectra, which allowed us to determine reorientation angles of $^{13}C$ and $^{15}N$ CSA tensors *using* the flip motion. In combination with the knowledge about fast averaging of the CH and NH heteronuclear dipolar couplings by the flip, this yields full information of the CSA tensor orientations in the molecular frame. Clearly, this approach is only possible when a well-defined molecular jump process exists, which can be probed all the way from the rigid to the fast limit. The

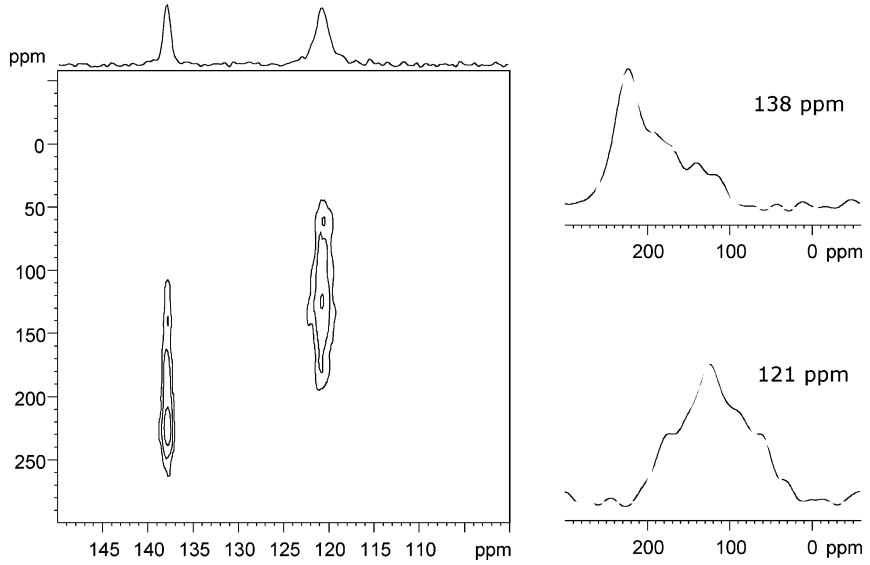


**Figure 6.** $^{13}$C−SUPER spectrum measured at $T = 355$ K. On the right, slices for the apical and the basal carbons are shown. Clearly, both patterns are not significantly changed as compared to the patterns measured at $T = 265$ K, as becomes clear when comparing to the underlying gray lines, which are the weblab simulations for the apical and the basal carbon from Figure 2.

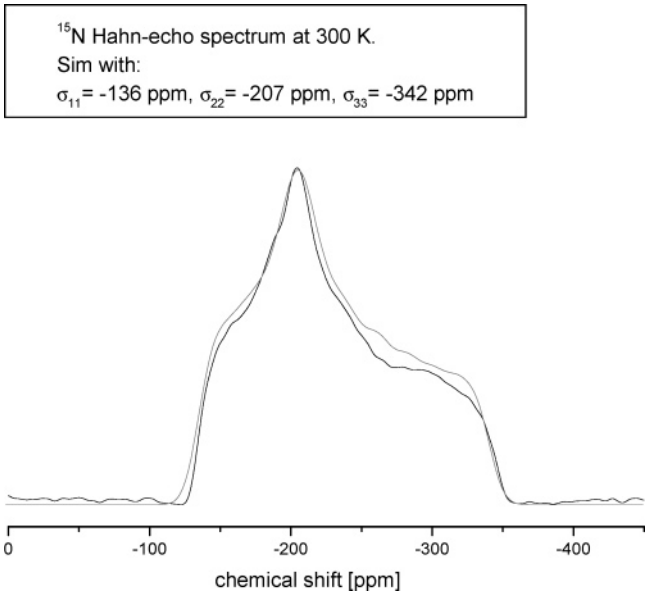


**Figure 7.** $^{15}$N Hahn echo spectrum measured at 303 K. The gray pattern is a calculated spectrum with the tensor values indicated in the figure.

approach certainly is not effortless, considering that the jump motion needs to be well characterized, for example, by CODEX. But, it needs to be compared to either variable-angle single-crystal or dipshift experiments, where in both cases selective isotope labeling is almost inevitable, as they are performed in static samples. Our determinations involving $^{13}$C are entirely performed on a powdered sample in natural abundance. Considering the large number of molecules in which flip motions are known to occur,[18,19] we nevertheless expect this approach to be of future use.

To return to the question of the importance of ring flips in proton transport mechanisms, we note that not only is the activation energy for the imidazolium ring flip comparable to activation energies in related imidazole compounds, but now, understanding the geometry of the ring flip, we can make use of this knowledge in the design of polymeric proton conductors. For example, tethering the imidazole ring from the apical position allows for the most efficient $C_2$ axis ring reorientation. It would be interesting to contrast this behavior with the well-established polybenzimidazole, in which such a ring reorientation is prohibited due to the bonding geometry.

**(c) Proton Conductivity in Pristine Imidazole.** Of course, when studying proton-conductivity phenomena in imidazole-based materials, the obvious candidate as a model system is imidazole itself. There have been several studies of imidazole, dating back to single-crystal investigations of conductivity as a function of crystal axis coordinates.[30] The conclusions of this early work was that conductivity occurred preferentially along the *c* axis, or hydrogen-bonding axis of the crystal. Since then, researchers have probed the crystalline phase using 2D-Exchange NMR, with the aim of detecting $^{15}$N exchange cross-peaks, which would confirm ring reorientation.[24,25] The two studies in the literature present negative results. We note, however, that both these studies were based on cross-polarization transfer of magnetization from $^{1}$H to $^{15}$N, and therefore selected against any mobile protons. The first study utilized static 2D $^{15}$N Exchange and the second studied the same system using CP/MAS. In both cases, no evidence of cross-peaks between the two $^{15}$N sites was observed.

Also, researchers have investigated the ring-flip process by studying diffusion of an excess proton in an imidazole chain using ab initio molecular dynamics simulations. In this study, the diffusion mechanism was determined to be structural, and, moreover, the ring reorientation step was found to be rate limiting.[14] These results are in good agreement with our findings.

We observe that single-pulse excitation of $^{15}$N-labeled imidazole under ambient temperature bearing gas and 30 kHz MAS, or a 330 K sample temperature (well below the melting point of imidazole), gives spectra such as Figure 9, where the bottom spectrum was acquired with a recycle delay of 180 s and those above were acquired with a recycle delay of 2 s. The difference between these spectra gives a clear indication of the relatively short $T_1$ of the resonance observed in the above spectra, as compared to those in the bottom spectrum. The important feature of these spectra is that only the outer resonances, at $\delta = 134$ and $\delta = 208$ ppm, produce signals under cross-polarization, whereas the center resonance represents $^{15}$N sites in fast exchange and is absent from the spectrum acquired under cross-polarization . The center resonance is assigned to imidazole rings undergoing fast exchange about the $C_2$ axis of the molecule. These spectral signatures are characteristic of our earlier $^{1}$H

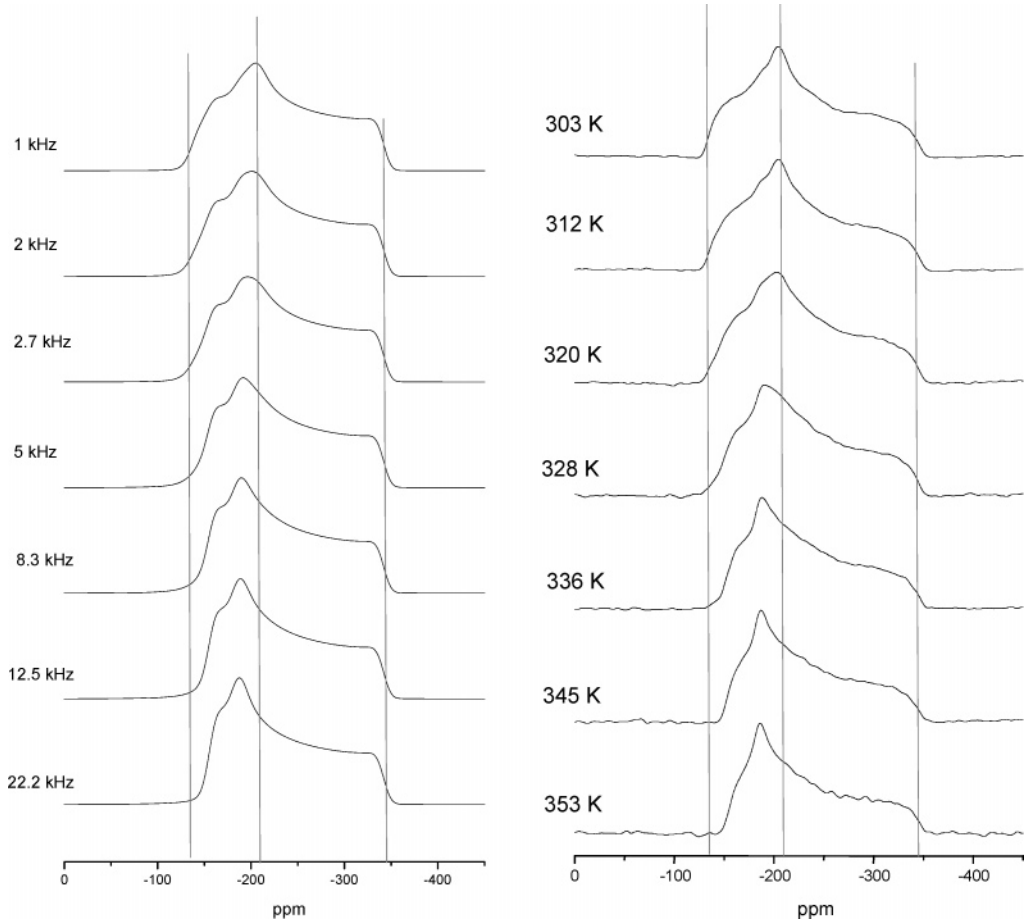


**Figure 8.** $^{15}$N-static powder patterns at various temperatures. On the left, calculated spectra for correlation times extracted from the Arrhenius plot are shown. The trend in the experimental $^{15}$N spectra (right) is consistent with the trend in the theoretical spectra, proving that only one motional process is present over the various decades.

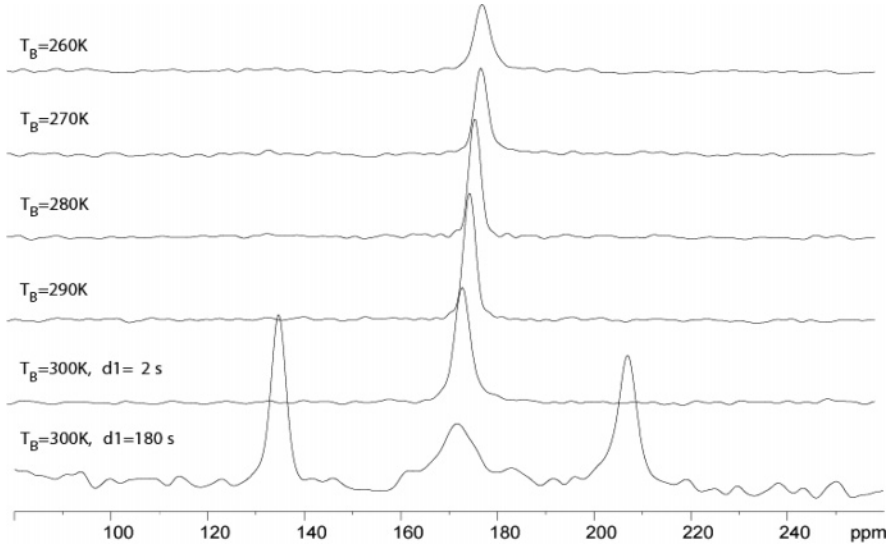


**Figure 9.** Temperature dependent $^{15}$N MAS spectra of pristine imidazole at a $^{15}$N Larmor frequency of 70.93 MHz. Marked temperatures indicate bearing gas temperature. For the first spectrum, the spinning speed was 8 kHz, the recycle delay was set to 120 s, and the number of scans was 16. For the above spectra, the spinning speed was 30 kHz, the recycle delay was set to 2 s, and the number of scans was 256 for each spectrum.

NMR studies of imidazole, in which both rigid and mobile hydrogen-bonded protons are observed, as indicated by their respective chemical shifts, $\delta_{\text{rigid}} = 14.6$ ppm and $\delta_{\text{mobile}} = 12.0$ ppm, their relative spin−lattice relaxation times, and their response to a double quantum filter.[6] As was observed for other imidazole-based materials, the mobile proton resonances are removed by the DQ sequence, due to their averaged dipolar couplings, as illustrated in Figure 10. While there is a trace of the lower frequency N−H resonance in the DQ-filtered spectrum, our attempts to enhance the strength of the signal by increasing the recoupling time, or to correlate this resonance to the rest of the spectrum using 2D DQF methods, have been unsuccessful. We hypothesize that these protons arise from mobile or disordered domains, which nevertheless retain some

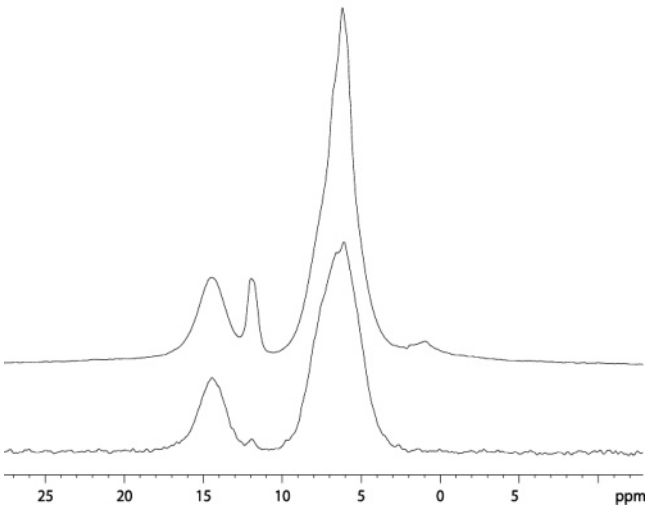


**Figure 10.** $^{1}$H MAS spectra of pristine imidazole at a $^{1}$H Larmor frequency of 500.13 MHz, under 30 kHz MAS. The top spectrum was acquired using a Bloch decay with 16 scans and a recycle delay of 120 s. The bottom spectrum was acquired using a back-to-back double quantum filter with two rotor periods of excitation, with 64 scans, and with a recycle delay of 120 s.

of their dipolar coupling, possibly due to some residual anisotropy in the defects, for example along the hydrogen bonding *c* axis of the crystallites.

To investigate this mobile phase further and, in particular, to probe the proposed anisotropic mechanism of proton conductivity in crystalline imidazole, a single crystal diffraction study was performed. Our aim was to detect possible defects, such as slip planes, or twinning, which would account for the early conductivity observations. Surprisingly, photographs taken of an imidazole single crystal during a diffraction study showed surface degradation, and after 24 h the crystal ($0.1 \times 0.2 \times 0.2$ mm) had evaporated at RT, under constant dry nitrogen flow. However, the crystal diffracted well throughout the diffraction study (8 h duration), indicating that the surface degradation process, which is presumed to create disordered regions at the surface of the crystal, was not affecting the crystallinity of the bulk sample. Thus, we conclude that the crystalline regions are not participating significantly in proton transport, rather it is mainly occurring in such disordered regions and at grain boundaries.

We have carried out $^{15}$N variable temperature measurements, as shown in Figure 9, in which a clear narrowing of the mobile resonance with increasing temperature is accompanied by increasing intensity. Clearly, the relative amount of the disordered phase can be controlled simply by varying the temperature of the samples. In the temperature range 260−300 K (bearing gas), the $^{15}$N chemical shift of the central resonance changes by 5 ppm, which can be attributed to the changing hydrogen bonding strength in the mobile domains. This is comparable to the behavior of the Imi-nEO materials, in which the chemical shift of the mobile protons was observed to change its frequency as the hydrogen bonding in the mobile domains became more dynamic.[6] Also, a static $^{15}$N NMR measurement of this resonance produced only a comparably narrow resonance, at the isotropic chemical shift, with no evidence of anisotropy. These results indicate that this mobile phase is isotropic in nature and lacks a strong preferred orientation, consistent with the diffraction study.

These observations, combined with the $^{1}$H DQ NMR and $^{15}$N data, indicate that proton conductivity in imidazole itself occurs via amorphous grain boundaries in which the activation energy for ring reorientation is lowered and hydrogen bonding is dynamic. This picture matches very closely to the model developed for proton conductivity in Imi-nEO.[6] It is also consistent with impedance spectroscopy measurements of macroscopic proton conduction, in which an abrupt change in the slope of conductivity versus temperature is observed above the melting transition, that is, above the temperature where grain boundaries inhibit long-range proton transport. We therefore propose that the earlier study of conductivity in a large imidazole single crystal was somewhat misleading, due to the likely presence of defects in such a large crystal. While proton conductivity certainly occurs via the breaking and reforming of hydrogen bonds, the concerted reorientation of otherwise rigid rings along a crystal axis is unlikely, and a more plausible scenario involves the presence of defects, grain boundaries, and amorphous domains.

## Conclusions

We have now fully characterized the two-site ring reorientation process in imidazolium methylsulfonate, using several complementary NMR methods. This ring flip is found to have an activation energy of $63.7 \pm 5$ kJ/mol, by combining data from $^{13}$C coalescence, $^{13}$C REPT, and $^{13}$C CODEX measurements. This value is an improved estimate of the energy barrier, compared to our earlier report, for which the CODEX data was not available. We have established the tensor elements and orientations of both the $^{13}$C and $^{15}$N nuclei and used these to confirm the single motional process acting in this material. Also, the CODEX recoupling-time-dependent build up curve was analyzed using the $^{13}$C CSA information from the SUPER experiment.

Also, we have shown that well-defined molecular processes, for example, those that can be characterized by CODEX, can be used to deduce or confirm tensor orientations for heteronuclei such as $^{13}$C and $^{15}$N in materials that possess local order.

We have provided new insight into the proton-conductivity mechanism in imidazole itself. We have determined the similarity between proton mobility in this material and that established for Imi-nEO. In both cases, conductivity occurs in amorphous, disordered domains, in which dynamic hydrogen bonding is possible, as observed here through both $^{1}$H and $^{15}$N NMR.

Most significantly, we have established the activation energy for the ring reorientation process in imidazolium methylsulfonate, which correlates well with the activation energies for proton mobility in imidazole-based proton conductors such as Imi-nEO. The differences between the values can be attributed to the relative strengths of the electrostatic interactions and steric constraints involved.

**Acknowledgment.** Financial support from the DFG and NSERC is acknowledged. The authors wish to thank Dr. Daniel Sebastiani and Dr. Ingo Schnell for helpful discussions, and Dr. Martin Schuster for providing the sample.

## References and Notes

(1) Kreuer, K. D. *Chem. Mater.* **1996**, *8*, 610−641.
(2) Schuster, M.; Meyer, W. H.; Wegner, G.; Herz, H. G.; Ise, M.; Schuster, M.; Kreuer, K. D.; Maier, J. *Solid State Ionics* **2001**, *145*, 85−92.
(3) Schuster, M. F. H.; Meyer, W. H. *Annu. Rev. Mater. Res.* **2003**, *33*, 233−261.
(4) Bozkurt, A.; Meyer, W. H.; Gutmann, J.; Wegner, G. *Solid State Ionics* **2003**, *164*, 169−176.
(5) Carrette, L.; Friedrich, K. A.; Stimming, U. *ChemPhysChem* **2000**, *1*, 162−193.
(6) Goward, G. R.; Schuster, M. F. H.; Sebastiani, D.; Schnell, I.; Spiess, H. W. *J. Phys. Chem. B* **2002**, *106*, 9322−9334.

(7) Goward, G. R.; Saalwachter, K.; Fischbach, I.; Spiess, H. W. *Solid State NMR* **2003**, *24*, 150−162.

(8) *Proton Conductors: Solids, Membranes, and Gels − Materials and Devices*; Colomban, Ph. Ed.; Cambridge University Press: Cambridge, 1992.

(9) McFarlane, D.; Huang, J.; Forsyth, M. *Nature* **1999**, *402*, 792−794.

(10) Forsyth, M.; MacFarlane, D. R.; Golding, J. J.; Huang, J.; Sun, J.; Forsyth, M. *Chem. Mater.* **2002**, *14*, 2103−2108.

(11) Forsyth, M.; Huang, J.; MacFarlane, D. R. *J. Mater. Chem.* **2000**, *10*, 2259−2265.

(12) Flakus, H. R.; Bryk, A. *J. Mol. Struct.* **1995**, *372*, 215−227.

(13) Sebastiani, D.; Goward, G.; Schnell, I.; Parrinello, M. *Comput. Phys. Commun.* **2002**, *147*, 707−710.

(14) Munch, W.; Kreuer, K. D.; Silvestri, W.; Maier, J.; Seifert, G. *Solid State Ionics* **2001**, *145*, 437−443.

(15) Saalwächter, K.; Spiess, H. W. *J. Chem. Phys.* **2001**, *114*, 5707−5728.

(16) Saalwächter, K.; Graf, R.; Spiess, H. W. *J. Magn. Reson.* **2001**, *148*, 398−418.

(17) deAzevedo, E. R.; Hu, W.-G.; Bonagamba, T. J.; Schmidt-Rohr, K. *J. Chem. Phys.* **2000**, *112*, 8988−9001.

(18) Reichert, D.; Hempel, G.; Zimmermann, H.; Schneider, H.; Luz, Z. *Solid State NMR* **2000**, *18*, 17−36.

(19) Fischbach, I.; Pakula, T.; Minkin, P.; Fechtenkotter, A.; Müllen, K.; Saalwächter, K.; Spiess, H. W. *J. Phys. Chem. B* **2002**, *106*, 6408−6418.

(20) Wind, M.; Saalwächter, K.; Wiesler, U.-M.; Müllen, K.; Spiess, H. W. *Macromolecules* **2002**, *35*, 10071−10086.

(21) Liu, S.-F.; Mao, J−D.; Schmidt-Rohr, K. *J. Magn. Reson.* **2002**, *155*, 15−28.

(22) Spiess, H. W.; Schmidt-Rohr, K. *Multidimensional Solid-State NMR and Polymers*; Academic Press: London, 1994.

(23) Solum, M. S.; Altmann, K. L.; Strohmeier, M.; Berges, D. A.; Zhang, Y.; Facelli, J. C.; Pugmire, R. J.; Grant, D. M. *J. Am. Chem. Soc.* **1997**, *119*, 9804−9809.

(24) Hickman, B. S.; Mascal, M.; Titman, J. J.; Wood, I. G. *J. Am. Chem. Soc.* **1999**, *121*, 11486−11490.

(25) Ueda, T.; Masui, H.; Nakamura, N. *Solid State NMR* **2001**, *20*, 145−155.

(26) Saalwächter, K.; Schmidt-Rohr, K. *J. Magn. Reson.* **2000**, *145*, 161−172.

(27) Benhabbour, S. R.; Goward, G. R. Presented at the Experimental NMR Conference; Asilomar, CA, 2004.

(28) Veeman, W. S. *Prog. Nucl. Magn. Reson. Spectrosc.* **1984**, *16*, 193−235.

(29) Sebastiani, D. unpublished results and private communication.

(30) Kawada, A.; McGhie, A. R.; Labes, M. M. *J. Chem. Phys.* **1970**, *52* 3121−3125.

(31) Macho, V.; Brombacher, L.; Spiess, H. W. *Appl. Magn. Res.* **2001**, *20*, 129−135.